RSC Advances

ROYAL SOCIETY OF CHEMISTRY

www.rsc.org/advances

RSC Advances

ARTICLE

Targeting chemorefractory COLO205 (BRAF V600E) cell lines using substituted benzo[α]phenoxazines†

Sanjima Pal[a], V Badireenath Konkimalla*[a], Laxmi Kathawate[b], Soniya S. Rao[b], Shridhar P. Gejji[b], Vedavati G. Puranik[c], Thomas Weyhermüller[d] , Sunita Salunke-Gawali*[b]

Received 00th January 20xx,
Accepted 00th January 20xx
DOI: 10.1039/x0xx00000x
www.rsc.org/

Mutational activation of oncogene *BRAF* (especially BRAF V600E) lacks proper prognosis in colon cancer patients and associated with chemoresistance rendering them refractory to treatment. Development of novel bioactive compounds with specific targeting abilities under such conditions is a need of hour in drug discovery. In this report we synthesized and characterized three fluorescent benzo[α]phenoxazines compounds (10R-benzo[α]phenoxazine-5-one, **1B**; R=Cl, **2B**; R= CH_3, **3B**; R=H) and their anticancer activity was evaluated in COLO205 cell line. All three compounds with a logP value around 2 were cell permeable. However, **2B** and **3B** showed specific cytotoxicity in malignant COLO205 cell line with BRAF mutation (V600E) in comparison to non-malignant wild-type BRAF HEK293T cell line. From further cell based assays (cell cycle analysis, DNA fragmentation and caspase activation), we conclude that **2B** and **3B** treatment induced selective cell death by inducing cell cycle arrest at G0/G1 phase and caspase-mediated apoptosis (activation of intrinsic and extrinsic pathways) only in BRAF V600E COLO205 cells. Further studies in the drug discovery pipeline might help developing these benzo[α]phenoxazines as a promising chemotherapeutic in such refractory mutated cancers.

Introduction

RAS and RAF kinases are the integral parts of the RAS-RAF-MAP2K (MEK)-MAPK signalling pathway that responds to several growth factors and cytokines. [1-3] There are several reports available indicating the importance of aberrantly functional KRAS and BRAF in tumor maintenance.[2, 4-6] Despite having a common activator (Ras) and substrate (MEK), the BRAF isoform has the highest activity among its three isoforms (A-,B- and C-RAF).[7-10] A specific point mutation (c.1799T->A) BRAF V600E within the kinase activation domain of the BRAF protein is the most common BRAF mutation that constitutively activates substrate MEK eventually leading to development of several types of malignant and drug resistant cancers. [11-14]

Epidemiological studies demonstrate that almost 8% of all solid tumors including 50% of melanomas, 30-70% of papillary thyroid carcinomas and 5-8% of colorectal adenocarcinomas are associated with this particular V600E mutation.[15] A dramatic response rate was observed when malignant melanoma cells with BRAF V600E mutation was treated with vemurafenib (a BRAF V600E selective inhibitor), however, a low clinical response was observed in colon cancer patients bearing the same mutation[16-18]. Most colon cancer cells harboring such point mutation are highly metastatic and non-responsive to established treatment regime e.g., anti-EGFR mAb (cetuximab, panitumumab) and/or chemotherapeutic inhibitors (vemurafenib, sorafenib, or MEK inhibitors).[19-22] According to reports, colon cancer cells acquire such characteristics by adopting different mechanisms e.g. amplification or altered splicing of BRAF genes, altered status of EGFR.[13, 23-25] With no suitable biomarkers available till date, prognosis for BRAF V600E mutation in cancers is still elusive for the treatment of colorectal cancer with standard chemotherapeutic agents or anti-EGFR monoclonal antibodies.[20, 26-29] Therefore, understanding the importance and prevalence of V600E BRAF mutation in chemo resistant cancers there is a need to develop novel organic compounds that can cause cell death in a V600E BRAF mutated condition selectively.

In this context, the chemical structure of benzo[α]phenoxazine (BPZ) and its derivatives exhibits several interesting features to develop it as a suitable targeting molecule. Molecular docking studies with G-tetrad showed that the delocalized π-electrons from the planar BPZ core-group promoted stable π-stacking with G-tetrad of DNA[30]. Biophysical studies using SPR further confirmed its selective affinity to DNA secondary structures where BPZ binding to G-quadruplex

[a]*School of Biological Sciences, National Institute of Science Education and Research (NISER), Bhubaneswar 751005, Orissa. India; Email: badireenath@niser.ac.in*

[b]*Department of Chemistry, Savitribai Phule Pune University, Pune 411007, India; Fax: +912025693981 ; Tel: +912025601397 -Ext-531; E-mail: sunitas@chem.unipune.ac.in*
[c] *Center for Material Characterization, National Chemical Laboratory, Pune 411008, India*
[d]*MPI für Chemische Energiekonversion, Stiftstr. 34-36, 45470 Mülheim an der Ruhr, Germany*

†Electronic Supplementary Information (ESI) available: Characterization of **1B -3B** by HR-MS Figures (Fig.S1, Fig.S5, Fig.S9), FT-IR figures (Fig.S2, Fig.S6, Fig.S10), ^1H and ^{13}C NMR(Fig.S3, Fig.S7, Fig.S11), 2DgHSQCAD(Fig.S4, Fig.S8, Fig.S132), Cyclic voltammetry (Fig.S13). Crystallography figures (Fig.S14-Fig.S16) Crystallographic tables Table S1 to Table S8. CCDC numbers 1412950 for **2B** and 1413927 for **3B**.
See DOI: 10.1039/x0xx00000x

sequence in c-KIT promoter and reducing c-KIT expression in a human gastric carcinoma cell line was reported indicating its potential as an anti-tumor agent[31]. In a previous study, we reported the inhibitory activity of some BPZ derivatives on topoisomerases (DNA-binding enzymes)[32]. Apart from DNA binding, some derivatives of BPZ induced photocytotoxicity in murine sarcoma cells sensing the pH in the microenvironment and changing the redox status within the cell[33]. Further, the inherent fluorescent nature of these compounds and its ability to permeate cells has been shown to selectively localize in different cell organelles (mitochondria and golgi) enabling cell imaging studies[34]. This way BPZ derivatives offer a great advantage in cancer chemotherapy as threnostics where solid cancers can be specifically tracked and treated simultaneously.

In the current study, BRAF mutated colon cancer cell line, COLO205, that demonstrate all above mentioned treatment resistant characteristics was considered as a suitable model for screening new bioactive chemical entities in such mutated condition.[35,36] Here, three intrinsically fluorescent benzo[α]phenoxazines (10R-benzo[α]phenoxazine-5-one, **1B**; R=Cl, **2B**; R= CH_3, **3B**; R=H) were synthesized and characterized. Their anti-proliferative activity was assessed on an established BRAF mutation (V600E) harbouring colon cancer model, COLO205. These compounds being intrinsically fluorescent it enabled us to conduct further validation studies for its cellular uptake, distribution and dose-dependent activity effectively.

Scheme 1

Results and discussion

Synthesis

Benzo[α]phenoxazine derivatives **1B**, **2B** and **3B**, were synthesized by Michael addition of phenolic hydroxyl group of 4R-2-aminophenol(R= Cl;**1B**, -CH_3;**2B** and H;**3B**) to 2-hydroxy-1,4-naphthoquinone.[37] **1B**, **2B** and **3B** are the minor products of reaction between 2-hydroxy-1,4-naphthoquinone and derivatives. Reaction mechanism is presented in Scheme 2. The 1,4-Michael addition elimination of hydroxyl group of aminophenol to C(2) carbon of 2-hydroxy-1,4-naphthoquinone results in species (iv) and further 1,2-Michael addition of amino group of aminophenol on carbonyl carbon C(1) generates aminol as unstable intermediate (vi). Further dehydration of (vi) results in the final product **1B** to **3B**.

Scheme 2

Molecular mass and purity of the compounds were determined by HR-MS (Fig.S1, Fig.S5, Fig.S9 in ESI†). The frequency at 1647, 1639 and 1635 cm^{-1} in FT-IR spectra was assigned to $\nu_{C=O}$ vibration in **1B**, **2B** and **3B** respectively and $\nu_{C=N}$ frequency was assigned at 1573, 1587 and 1593 cm^{-1} respectively to **1B**, **2B** and **3B**. *Para*-naphthoquinone (p-NQ) vibration (~1280 cm^{-1}) in all compounds, however a peak due to $\nu_{C(6A)-O(7)}$ was observed ~1240, 1226, 1234 cm^{-1} in **1B**, **2B** and **3B** respectively. Chemical shifts were assigned by 2D gHSQCAD experiments (Fig.S4, Fig.S8 and Fig.S12 in ESI†). Unlike the quinone compounds, the benzo[α]phenoxazine derivatives **1B**, **2B** and **3B** were redox active (Fig.S13 in ESI†). The cyclic voltammogram of all the compounds showed one electron reversible redox couple at $E_{1/2}$ = 0.297 V, -0.379 V, -0.442 V for **1B**, **2B** and **3B** respectively in DMSO solution and the calculated logP (using chem sketch program) was determined to be 2.87, 2.79 and 2.33 respectively.

Single crystal X-ray diffraction studies of 2B and 3B

Compound **2B** and **3B** crystallizes in monoclinic space group $P2_1/n$. Fig.1 showed ORTEP plot and the crystallography parameters are presented in Table 1. The bond distance of C(5)=O(5) in both the compounds is ~1.23Å which typically falls to the oxidized form of quinonoid carbonyl.[32,37-39] After forming planar polycycles, both the compounds retain their quinonoid distortion in ring B (Scheme1) which was adjudge by the bond distances C=O and C=N.

Fig.1

X-ray structures **1B**, **2B** and **3B** formed dimer via C-H···O '*head to head*' (Table 2, Fig.S14 in ESI†) orientation of their respective molecules. Molecules of **2B** differed by slightly slipped C-H···O interaction. **2B** is in vicinity to nine neighbouring molecules (Fig.S15 in ESI†) via C-H···O and π-π stacking interaction, where as **3B** showed intermolecular hydrogen bonding to three neighbouring molecules via C-H···O interaction. Fig.2 showed molecular packing of **2B** and **3B** down b and a-axis respectively. A polymeric sheet of dimer molecules formed via C(3)-H(3)···O(5) interaction in both the compounds, in addition methyl group –C(13)H(13) took part in C-H···O interaction slipped π-π stacking is observed to **2B** molecules(Fig.S16 in ESI†). π-π stacking interaction is absent in compounds **1B** and **3B**. Compound **2B** differs with respect to π-π stacking interaction with the rest of the compounds **1B** and **3B**, this aspect could reflect the anticancer activity of these compounds.

Fig.2

Table 1

Table 2

Computational Studies

The structures of **1B**, **2B** and **3B** obtained from the present density functional theory are depicted in Fig.3. Selected bond distances (in Å) given along with. The structure obtained from the present theory is in consonant with single crystal data derived from X-ray diffraction experiments. To gain deeper insights for the charge distributions within these systems the molecular electrostatic potential (MESP) were computed within the same framework of theory. The MESP, V(r), results from the balance of bare nuclear and electronic contributions and brings about the effective electron-rich regions in the molecule. The MESP isosurfaces with V=−52.5 kJ mol^{-1} are compared in Fig. 3. As may readily be inferred the electron-rich regions are located near carbonyl oxygens in **1B-3B**. Furthermore the softness parameters (η) were computed from the difference of HOMO (Highest occupied molecular orbital) and LUMO (Lowest unoccupied molecular orbital) energies. Calculated η values for **2B** turns out to 0.109 eV, compared to that of 0.087 eV in **1B** and 0.015 eV in **3B**.

Fig. 3

Antiproliferative activity of 1B, 2B and 3B observed only in BRAF V600E colon cancer cells

The cell viability upon treatment with three compounds at varying concentrations in COLO205 (V600E BRAF, malignant)

and HEK293T (wild type BRAF, transformed non-malignant) showed that compounds **2B** and **3B** posses excellent anti-proliferative activity specifically in COLO205 with an IC_{50} value of 13 μM and 9 μM while for compound **1B** antiproliferative activity was observed only at concentrations above 50 μM (Fig. 5). No or negligible effect was observed in HEK293T cell line even when treated with doses as high as 100 μM (Fig.4). These data demonstrate that the compounds were able to induce cytotoxicity selectively in BRAF mutated colon cancerous cells and that the very significant activity of compounds **2B** and **3B** in comparison to **1B** indicates a strong structure activity relationship.

Fig.4

Compounds **1B, 2B** and **3B** with a substitution in -R for Cl, CH_3 and H is expected to be cell permeable with a logP value of 2.87, 2.79 and 2.33 respectively. As these compounds are innately fluorescent, flow cytometry and fluorescence microscopy were performed to study their cell permeability, retention and localization. From the analysis, only **2B** and **3B** were bioactive in COLO205 cells and others were inactive. Therefore, for all following studies in COLO205, **1B**, **2B** and **3B** were treated at 50 μM (high dose), 13 μM (IC_{50}) and 9 μM (IC_{50}) respectively and in HEK293T all compounds were treated at a high dose of 50 μM.

Comparative cell permeability of 1B, 2B and 3B

The excitation and emission wavelength of all three fluorescent compounds [**1B**: Ex-475 nm/Em-535 nm, **2B**: Ex-480 nm/Em-538 nm, **3B**: Ex-470 nm/Em-540 nm] were compatible for fluorescence microscopy and flow cytometry studies. From fluorescence microscopy studies, green fluorescence was detected following 15 min incubation with three compounds independently in both cell lines indicating cellular uptake in all cases. From DAPI stained nuclei, cytoplasmic accumulation of uptaken compounds was confirmed for all three compounds in both the cell lines (Fig. 5).

Fig.5

Under similar dose conditions, cellular uptake was quantified by flow cytometry following incubation with compounds under study for 15 min, 2 h and 24 h. From the results a differential cellular uptake was observed for the compounds in both cell lines at different time points. **1B** being treated at a high dose of 50 μM still had very less uptake in both cell lines. **2B** and **3B** were treated in HEK293T at an IC_{50} concentration which approximately five times higher in COLO205 showed a relatively higher uptake of **2B** in HEK293T in comparison to COLO205 treated at IC_{50}. But, for compound **3B**, the uptake was almost the same at all time-points whether it was COLO205 treated at IC_{50} or HEK293T treated at 50 μM (Fig. 6). The cell viability assay and cellular uptake studies indicate poor uptake of **1B** to reach the intracellular cytotoxic threshold concentration as a possible reason for its less potent antiproliferative activity. For **2B** and **3B** the treated doses and cellular uptakes in COLO205 were low in comparison to HEK293T still these two compounds were very cell permeable and able to effectively inhibit proliferation of COLO205 by 50%. Taking together these results we concluded that **2B** and **3B** are highly selectively for malignant COLO205 cells and that the cellular environment in the V600E BRAF mutated cancerous condition is responsible for its antiproliferative activity. Further, in order to understand in much detail the mechanistic activity for this selective cell death, studies for cell cycle arrest and apoptotic activity were performed for these compounds.

Fig.6

1B, 2B and 3B induced cell cycle arrest in BRAF V600E-COLO205

Post 24 h exposure with compounds, cell cycle analysis using flow cytometry showed a significant number of cells arrested at G_0/G_1 phase only in COLO205 cells treated with **1B**, **2B** and **3B** (Fig.7). Although HEK293T cells were treated at high doses, their cell cycle progression seems unaffected post 24h treatment (Fig.7). Apart from cell cycle arrest at G_0/G_1 phase a concomitant accumulation of sub G_1 population was observed that increased after 24h treatment which may be either due to apoptosis or necrosis. So further experiments were performed to elucidate the preferred cell death pathway (apoptosis or necrosis) induced by these compounds.

Fig.7

1B, 2B and 3B induce apoptosis in V600E BRAF colon cancer cells

Altered or deregulated apoptosis is reported in almost all tumor cells with significant role in promoting malignancy. To assess the apoptosis promoting ability of these compounds at the determined doses we studied the appearance of various apoptotic hallmarks (increment of annexin V positive cells, chromosomal DNA fragmentation and active or cleaved Caspase-3 accumulation) in treated cells at various times points after treatment.

Within 2h post treatment in COLO205 cells, these compounds showed an increased amount of annexin V positive cells due to alteration the membrane asymmetry and as an indicator for early marker of apoptosis (Fig. 8). From 24h treatment, an increase in the percentage of annexin-V positive and 7AAD/annexin-V double positive cells was observed only in COLO205 cells indicating severe cell death (data not shown). But treated HEK293T cells remained unaffected even after 24h treatment at high doses.

Fig.8

This increased 7AAD/annexin-V double positive cells due to cell death was further confirmed by DNA fragmentation assay, a late marker of apoptosis to establish the compounds as potential pro-apoptotic agents.

DNA fragmentation as an inference for late marker of apoptosis following 48h treatment was observed only in COLO205 even at very low doses (except **1B**). No fragmented chromosomal DNA (apoptosis) or smear (necrosis) was observed in treated HEK293T cell lines. These results confirmed that tested compounds are potent apoptosis inducers selective for malignant BRAF V600E colon cancer cells and non-malignant BRAF-WT cells will be unaffected by their treatment (Fig. 9).

Fig.9

1B, 2B and 3B induced caspase-dependent apoptosis in V600E COLO205 cells

To further investigate the mode of apoptosis in COLO205 cells, western blotting experiment was performed to detect active caspase-3 (cleaved) following 12h treatment with these

compounds. Appearance of cleaved caspase-3 is a hall mark for caspase-dependent apoptosis. In our experiment, the accumulation of the distinct, active as well as cleaved form of caspase-3 had been observed only in **1B**, **2B** and **3B** treated COLO205 cell lysate while active form of this executioner pro-apoptotic protein was absent in **1B**, **2B** and **3B** treated HEK293T cell lysates (Fig. 10).

Fig.10

For these experiments we could conclusively state that **1B**, **2B** and **3B** despite being cell permeable were selective in inducing cytoxicity in BRAF-V600E colon cells by causing cell cycle arrest accompanied by a caspase-dependent apoptotic pathway.

Conclusions

In the era of personalized medicine, single treatment or individualized treatment strategy against BRAF mutated colon cancer and other adaptive resistant cancer cells are not available due to harboring of different treatment refractory mutations. A very few p.BRAF V600E targeted inhibitors (e.g vemurafenib) are currently in different stages of clinical trials against melanomas but their efficacy is very low in similarly mutated colon cancer cells due to extremely poor clinical responses. Moreover from recent clinical studies, many cases of acquired resistance to vemurafenib have also been reported [40].

In the present study, we report cellular uptake of all three fluorescent compounds in both cell lines, but antiproliferative activity was observed in BRAF-V600E mutated colon cancer cell line, COLO205 when treated with **2B** and **3B**. Further detailed studies confirmed cell cycle arrest (G_0/G_1) and induction of caspase-dependent apoptosis to be the possible mechanism for the antiproliferative activity of **2B** and **3B**. Apart from potent anti-proliferative activity, a high degree of specificity for BRAF mutated cancer was also observed with **2B** and **3B** where both this compounds showed bioactivity only in malignant cancer colon cancer cells and had very minimal effect on the normal cells only at very high concentrations.

Another observation we report from our studies is that although one of the substituted benzo[α]phenoxazine **1B** was inactive in such BRAF mutated condition still it did not show any cytotoxic activity to the normal HEK293T cells at high concentration (same as the case with nor **2B** and **3B**) unlike other anticancer drugs (doxorubicin or staurosporin) that were used as positive control. This is an important prerequisite while developing any chemotherapeutics to address specificity and avoid cross reactivity making such class of compounds attractive for further studies. More studies exploiting the fluorescent nature of these compounds or their prototypes can be used in developing novel fluorophores for live imaging studies in animal models that would help in validating and establishing this class of compounds as potential anticancer agents against treatment refractory mutations and individualized treatment against colon cancer.

Experimental Section

Materials for chemical synthesis

All the chemicals used in synthesis are of analytical grade. Lawsone (2-hydroxy-1,4-napthoquinone) and 2-aminophenol has been obtained from Sigma-Aldrich and recrystallized from dry methanol before use. 4-chloro-2-aminophenol and 4-methyl-2-aminophenol were obtained from across chemicals. Anhydrous methanol used in the synthesis has been purified by literature reported procedure[41].

Synthesis of 1B to 3B

Recrystallized 2-hydroxy-1,4-naphthoquinone (lawsone) 1 mM (174 mg) was dissolved in 20 ml dry methanol. The solution was stirred for 15 min. The solids of 4-chloro-2-aminophenol, 1 mM (143 mg) in **1B**, 4-methyl-2-aminophenol 1 mM (123 mg) in **2B**, 2-aminophenol; 1 mM (109 mg) in **3B**, were dissolved in 10 ml dry methanol. The aminophenol solutions were added drop wise in to the solution of lawsone. The colour of reaction mixture turned from yellow to brown. The mixture was stirred at room temperature (26 °C) for 24 hrs in **3B** and refluxed for 62 hours in **1B** and **2B**. The reaction was monitored on TLC (9.5:0.5; toluene: methanol). Dark red colour products obtained were filtered and washed with small amount of methanol and dried in vacuum and purified by column chromatography. Fluorescent yellow band was separated as minor product for **1B** to **3B** with ~ 10% yield, while dark red band was separated as major product (**1A** to **3A**) by column chromatography(Scheme 3).

Scheme 3

FT-IR, Elemental Analysis, ^{1}H, ^{13}C and 2D gHSQCAD NMR, LC-MS, HR-MS, Cyclic Voltammetry studies

The FT-IR spectra of the compounds were recorded between 4000-400 cm^{-1} as KBr pellets on SHIMADZU FT 8400 Spectrometer. The elemental analyses were performed on Thermo Finnigan EA 1112 Flash series Elemental Analyzer. ^{1}H, ^{13}C and 2D gHSQCAD NMR of **1B** to **3B** were recorded in $CDCl_3$, on Varian Mercury 500 MHz NMR spectrometer with TMS (tetramethylsilane) as a reference. UV-Vis spectra of compounds are recorded on SHIMADZU UV 1650 in methanol between 200 to 800 nm. HR-MS spectra were recorded on Bruker impact HD with ESI source.

The electrochemical measurements were performed with CHI 6054E electrochemical analyser. A commercial Pt disc electrode (CHI Instruments, USA, 2 mm diameter), $AgNO_3$ wire and Pt wire loop were used as working, reference and counter electrodes respectively. After fixing the electrodes to the cell 0.513 g of tetra butyl ammonium perchlorate (100 mM in 15 mL solution) was transferred to the cell through high purity argon gas. The blank or controlled voltammograms were acquired in tetra butyl ammonium perchlorate–DMSO mixture prior to the measurements. Sample dispersed in small amount of solvent injected in the cell for further measurement (analytic concentration 5 mg/15 mL). At the end of each set of experiments the potentials were calibrated with respect to the normal hydrogen electrode (NHE) using ferrocene as an internal standard.

10-chloro-benzo[α]phenoxazine-5-one; 1B. Color: Orange solid, Yield: 28 mg (10%). m.p. 237 °C. FT-IR (KBr; cm^{-1}): 3064, 1722, 1647, 1624, 1573, 1273, 1240. ^{1}H NMR ($CDCl_3$, 125 MHz) δ/ppm: 8.701 (d, *J* = 7.5 Hz, 1H, Ar), 8.295 (d, *J* = 8.5 Hz, 1H, Ar), 7.796 (m, 2H, Ar), 7.437 (d, *J* = 8.5 Hz, 1H, Ar), 7.265 (d, *J* = 6.5 Hz, 1H, Ar), 7.835 (1H, s), 6.449 (s, 1H, Ar). ^{13}C NMR ($CDCl_3$, 125 MHz) δ/ppm: C(1) = 125.11, C(2) =132.45, C(3) = 132.53, C(4) = 126.24, C(4A) = 132.25, C(5) = 184.06, C(6A) =151.06, C(6) =108.12, C(7A) = 133.64, C(8) =117.20, C(9) =131.40, C(10) =130.36, C(11) =129.41,

C(11A) = 142.88, C(12A)= 148.76, C(1**2B**) = 131.17. UV-Vis; (DMSO, λ_{max}/nm): 280, 350, 438. LC-MS (*m/z*): 282 [M+1]. HR-MS (*m/z*): 282.0318. Anal. data calc. for $C_{16}H_8ClNO_2$ (281.69 g): C, 68.22; H, 2.86, N, 4.97 %. Found: C, 68.17; H, 2.93, N, 4.73 %.

10-methyl-benzo[α]phenoxazine-5-one; 2B. Color: Orange solid, Yield: 26 mg (10%). m.p. 201 °C. FT-IR (KBr; cm^{-1}): 3045, 1635, 1587, 1575, 1226. ^{1}H NMR ($CDCl_3$, 125 MHz) δ/ppm: 8.680 (d, *J* = 8.0 Hz, 1H, Ar), 8.276 (d, *J* =7.0 Hz, 1H, Ar), 7.731 (m, 2H, Ar), 7.269 (d, *J* = 9.0 Hz, 1H, Ar), 7.179 (d, *J* = 8.0 Hz, 1H, Ar), 7.601 (s, 1H, Ar), 6.399 (s, 1H, Ar), 2.438 (s, 3H,). ^{13}C NMR ($CDCl_3$, 125 MHz) δ/ppm: C(1) = 124.85, C(2) = 131.93, C(3) =132.12, C(4) =126.07, C(4A)= 132.75, C(5) =184.11, C(6A) = 151.63, C(6) =107.29, C(7A) = 135.38, C(8) = 115.67, C(9) = 132.66, C(10) =131.49, C(11) =130.01, C(11A) =142.25, C(12A) =147.43, C(1**2B**) =132.36. UV-Vis; (DMSO, λ_{max}/nm): 282, 357, 446. LC-MS (*m/z*): 262 [M+1]. HR-MS (*m/z*): 262.0863. Anal. data calc. for $C_{17}H_{11}NO_2$ (261.28 g): C, 78.14; H, 4.24, N, 5.36 %. Found: C, 78.23; H, 4.11, N, 5.28 %.

Benzo[α]phenoxazine-5-one; 3B. Color: Orange solid, Yield: 25 mg (10%). m.p. 191 °C. FT-IR (KBr; cm^{-1}): 3063, 1720, 1668, 1639, 1593, 1564, 1263, 1234. ^{1}H NMR ($CDCl_3$, 125 MHz, δ/ppm): δ: 8.696 (d, *J* = 7.0 Hz, 1H, Ar), 8.274 (d, *J* =8.0 Hz, 1H, Ar), 7.808 (d, *J* = 8.0 Hz, 1H, Ar), 7.766 (m, 2H, Ar), 7.475 (t, *J* = 8.0 Hz, 1H, Ar), 7.344 (t, *J* = 7.7, 1H, Ar), 7.260 (d, *J* = 8.0, 1H, Ar), 6.419 (s, 1H, Ar). ^{13}C NMR ($CDCl_3$, 125 MHz) δ/ppm: C(1) = 124.92, C(2) = 132.05, C(3) =132.21, C(4) =126.11, C(4A)= 132.35, C(5) =184.16, C(6A) = 151.47, C(6) =107.58, C(8) = 116.10, C(9) = 131.73, C(10) = 125.45, C(11) =130.11, C(11A) =144.27, C(12A) =147.60, C(1**2B**) = 131.43. UV-Vis; (DMSO, λ_{max}/nm): 280, 355, 432. LC-MS (*m/z*): 248 [M+1]. HR-MS (*m/z*): 248.0705. Anal. data calc. for $C_{16}H_9NO_2$[0.5 H_2O] (256.25 g): C, 74.99; H, 3.93, N, 5.46 %. Found: C, 75.05; H, 4.36, N, 5.22 %.

X-Ray Diffraction studies

An orange single crystal of **2B** was coated with perfluoropolyether, picked up with nylon loops and mounted in the nitrogen cold stream of the Bruker APEX-II diffractometer. Graphite monochromated Mo-Kα radiation (λ= 0.71073Å) from a Mo-target rotating-anode X-ray source was used. Final cell constants were obtained from least squares fits of several thousand strong reflections. Intensity data were corrected for absorption using intensities of redundant reflections with the program SADABS.[42] The structure was solved readily by direct methods and subsequent difference Fourier techniques. The Siemens ShelXTL[43] software package was used for solution and artwork of the structures, ShelXL97[44] was used for the refinement. All non-hydrogen atoms were anisotropically refined and hydrogen atoms were placed at calculated positions and refined as riding atoms with isotropic displacement parameters.

Single crystals **3B** were grown by slow evaporation of the solution of methanol. Data was collected on SMART APEX-II CCD using Mo-Kα radiation (λ = 0.7107 Å) to a maximum θ range of 25.00°. Orange coloured needle like crystal of approximate size 0.38 x 0.09 x 0.04 mm^3 was used for data collection. Crystal to detector distance 5.00 cm, 512 x 512 pixels / frame, Oscillation / frame -0.5º, maximum detector swing angle = –30.0º, beam center = (260.2, 252.5), in plane spot width = 1.24, Multirun data acquisition. Total scans = 2, total frames = 657, exposure / frame = 10.0 sec / frame, θ range = 0.66 to 25.00 º, completeness to θ of 23.97 º, is 99.6 %. C16 H9 N O2, *M* = 247.24. Crystals belong to Monoclinic, space group $P2_1/n$, *a* = 3.91910(9), *b* = 23.3060(5) Å, c = 12.3580(3) Å, *V* = 1125.56(4) $Å^3$, *Z* = 4, D_c = 1.459 g /cc, μ (Mo–Kα) = 0.097 mm^{-1}, 7783 reflections measured, 1766 unique [I>2σ(I)], R value 0.0350, wR2 = 0. 0901. Largest diff. peak and hole 0.176 and -0.128 e. $Å^{-3}$. All the data were corrected for Lorentzian, polarisation and absorption effects. SHELX-97 (ShelxTL)[43,44] was used for structure solution and full matrix least squares refinement on F^2. Hydrogen atoms were included in the refinement as per the riding model and refined. Data collection and refinement parameters are listed in Table 1.

Computational Methodology

The optimized structures of **1B**, **2B** and **3B** were obtained within the framework of M06-2x[45,46] density functional theory using the Gaussian-09 program.[47] The internally stored 6-31++G (d,p) basis with the diffuse functions being added on the heavy atoms has been employed.[45-47] The structures were confirmed to be local minima on the potential energy surface through vibrational frequency calculations. .

Chemical and reagents for bioactivity studies

Stock solutions of **1B, 2B** and **3B** were prepared at a concentration of 20 mM in DMSO [MP Biomedicals, #196055] and stored at -20°C. Chemicals and reagents used in the experiments XTT (2,3-bis-(2-methoxy-4-nitro-5-sulfophenyl)-2H-tetrazolium-5-carboxanilide) (#158788), PMS N-methyl dibenzopyrazine methylsulfate (#194595), doxorubicin (#159101) RNaseA (#0107680), proteinase K(#9398125), propidium iodide (#19545810), phenol: chloroform saturated solution, pH 6.7 (#154903), EDTA (#194822), triton X-100 (Cat No: 194854), DAPI(#15757405) ethidium bromide (EtBr, #802511), polysorbate 20 (Tween-20, #103168), SDS (#102918), protease inhibitor cocktail (#158837) were procured from MP Biomedicals. Buffers and media such as 10X PBS (#ML023), DMEM (#AL007A), RPMI (#AL162S), Foetal Bovine Serum (#RM9970) were purchased from HIMEDIA while Tris-HCl (#T5941), Trizma base (#T1503), sodium chloride (#S3014) and methanol (#154903) were purchased from Sigma. Agarose for agarose gel electrophoresis was procured from Conda (#8012). Antibodies and reagents for performing western blotting were purchased from Cell Signaling (primary rabbit anti-human Caspase3 (#9665), anti-β-actin (#4970), secondary goat anti-rabbit HRP-IgG (#7074) and 20X lumiGLO® ECL reagent and 20X peroxide (#7003S). PVDF membrane (#1620177) and acrylamide/bisacrylamide solution 30% (29:1) (#1610156) were purchased from Bio-rad. Pre-stained protein ladder was bought from Fermentas (#SM0671) to perform SDS-PAGE.

Cell lines and culture conditions

Both human malignant colon cancer cell line, COLO205 (heterozygous for BRAF: c.1799T>A or p.V600E)17 and transformed, non-malignant human embryonic kidney cell line HEK293T (BRAF-wt and inactivated p53 by expressing SV40 large T antigen) were cultured in RPMI-1640 and DMEM growth medium respectively in an incubator maintained at 37°C with constant supply of 5% CO_2. All media were supplemented with 10% heat-inactivated fetal bovine serum (FBS), 1% L-glutamine

and 1% penicillin-streptomycin. During each experiment final FBS concentration was maintained at 5% in all growth medium.

***In vitro* cell viability assay**

A colorimetric assay using XTT was performed on both the cell lines (COLO205 and HEK293T) to study the effect of compounds **1B**, **2B** and **3B** on their cell proliferation activity. Briefly, 100 µL media containing $1x10^4$ cells were sown into each well of a 96-well plate and incubated for minimum 8h for cell adherence. Later, cells were incubated independently with increasing concentrations (10^{-8} to 10^{-4} M) of all three test compounds for 72h at 37°C in 5% CO_2 incubator. Each experimental 96-well plate had cells similarly treated with doxorubicin that served as positive control while cells treated with DMSO at a final concentration of 0.5% was used as solvent control. Duplicate wells were used for each treatment. Post incubation, 50 µL of assay mix consisting of XTT and PMS (49:1) were added to each well. After about 8h incubation, the enzymatic activity of mitochondrial dehydrogenase present in metabolically active cells cleaved XTT releasing an orange formazan dye. The intensity of coloured product formed is taken as a measure of the number of active cells present. Micro-plate reader (iMark, Biorad) was used to measure the intensity of absorbance from the coloured product formed by setting the wavelength at 490 nm with a reference wavelength at 655 nm. The percentage cell viability was calculated using the following equation,

Cell viability (%) = (O.D sample /O.D DMSO treated control) x 100

Where O.D sample is the intensity obtained from the cells incubated with the compounds at varying concentration and O.D DMSO treated control is the intensity of the cells incubated with 0.5% DMSO alone. Sigmoidal curves were plotted using Origin Pro software and IC_{50} concentrations of the test compounds were determined from the same.

Cellular permeability and localization studies using fluorescence microscopy

About $1x10^4$ cells of COLO205 and HEK293T cells were grown on cover slips placed in each well of a 24-well plate containing respective growth media. The cells in each well were then treated with the fluorescent test compounds **1B**, **2B** and **3B** at a final concentration (either at IC_{50} or a high dose of 50 µM) and incubated upto 24 h at 37°C under continuous flow of 5% CO_2. Post incubation, cells were washed twice with PBS and fixed with 2% paraformaldehyde. Cells were fixed and nuclei were counter stained with DAPI. Whole cell images were captured at 40X magnification using a fluorescence microscope (Olympus) applying appropriate wavelength filters.

Quantitative cellular uptake studies using flow cytometry

~$1x10^6$ of COLO205 and HEK293T cells were incubated with test compounds **1B**, **2B** and **3B** either at a final concentration of their IC_{50} or 50 µM in growth media at 37°C. Post-treatment, the cells were harvested after time points 15 mins, 2h and 24h followed by washing with ice cold PBS. Finally, single cell suspensions were prepared in 500 µL PBS to determine the mean fluorescence intensity at compensated FL1 voltage by flow cytometry using FACS-Calibur flow cytometer (BD Biosciences) using excitation and emission wavelengths compatible with the same channel for individual compounds [**1B**: Ex-475 nm/Em-535 nm, **2B**: Ex-480 nm/Em-538 nm, **3B**: Ex-470 nm/Em-540 nm]. 5000 gated live events were taken from the forward vs side scattering plots (ensuring the similar sizes and granularity in both treated as well as untreated conditions), to analyse the extent of compound uptake into the cells after each indicated time point. Histograms were obtained by comparing the mean fluorescence intensity of test samples with that of DMSO treated control samples.

Cell cycle analysis

Effect of **1B**, **2B** and **3B** on cell cycle progression was studied using flow cytometry (BD Biosciences). Briefly, post 24 h incubation with test compounds at IC_{50} or 50 µM with 10^6 cells/ml, the growth medium was discarded and cells were harvested with ice cold PBS and fixed in 3% paraformaldehyde before staining with mixture containing propidium iodide (PI), Triton X-100 and RNaseA. 5,000 live gated events were acquired using flow cytometer. Cell Quest Pro software was used to generate histograms based on the DNA content in each phase of cell cycle.

Annexin-V/7AAD assay

Annexin-V assay was carried out using flow cytometry to examine apoptosis induction on COLO205 and HEK293T cells in response to the treatment with the test compounds. Briefly, $1x10^6$ live cells were seeded into 24-well plates containing complete growth medium in the absence or presence of test compounds treated at IC_{50} or 50 µM and incubated at 37°C in 5% CO_2. After 2h and 24h treatment, cells were harvested and washed twice with ice cold PBS. Single cell suspensions were prepared in 1X binding buffer (BD biosciences). Staining was performed as per protocol mentioned in user's guide of Annexin V apoptosis detection kit (BD biosciences #559763). Gated population obtained from the scatter plots and cells undergoing apoptosis upon compound treatment were determined and represented in terms of percentage by comparing test samples with DMSO treated solvent control.

DNA fragmentation studies

COLO205 and HEK293T cells at a density of 10^6 cells/ml were sown into 65 mm dishes containing respective growth medium and incubated with test compounds at IC_{50} or 50 µM for 48h at 37°C in 5% CO_2. 0.5% DMSO treated cells was used as solvent control. Cells were lysed in lysis buffer containing 10 mM Tris-HCl (pH 8), 150 mM NaCl, 5 mM EDTA and 0.5% Triton X-100. Lysates were vortexed and incubated with 0.1 mg/ml RNaseA for 1h at 37˚C followed by proteinase K (0.1mg/ml) treatment for another 2h under same condition. Later the lysate was extracted for chromosomal DNA using phenol/chloroform/isoamyl alcohol mixture (25:24:1). The quantity and quality of DNA was assessed using Nanodrop spectrophotometer (Thermo Scientific) where quality (260:280) of extracted DNA was expected to be within a range of 1.8 – 2.0. Equal amounts (in terms of DNA content) of individual sample were loaded and electrophoresed on 1.8% agarose gel containing 0.1 µg/mL ethidium bromide to observe any fragmented chromosomal DNA.

Caspase-3 activation studies

About $1x10^6$ COLO205 and HEK293T cells were sown in 35 mm dishes in the presence or absence of test compounds and incubated for 12h at 37°C in 5% CO_2. Post treatment samples were harvested with ice cold PBS and simultaneously lysed with 50 mM Tris buffer pH 8.0, 150 mM NaCl and 1% Triton X-100 along with the cocktail of protease inhibitor and total protein concentration was measured at 280 nm nanodrop-2000, (Thermo scientific). Later each sample was boiled with equal amount of laemmli sample buffer (4% sodium dodecyl sulfate (SDS), 10% β-mercaptoethanol, 20% glycerol, 0.004% bromophenol blue, 0.125M Tris-Cl pH-6.8). Along with pre-stained protein loading marker, 20 µL samples containing equal amount of proteins were separated electrophoretically in 10% SDS-PAGE. Upon proper separation of bands as observed from the marker, the resolved proteins were electroblotted from the gel to methanol pre-activated PVDF membrane using semidry blotter (Biorad). The protein transferred PVDF membranes were incubated with blocking buffer (5% skimmed milk in TBST) for 1hr at room temperature on a rocker. The membranes were then incubated overnight with primary antibody (anti-human caspase-3 and β-actin, both at 1:1000 dilutions. Following incubation with primary antibody, the membranes were washed twice with TBST (Tween-20 in Tris-buffered saline) and once with TBS (without Tween-20) before incubation with secondary anti-rabbit HRP-IgG (goat) for next 1h at room temperature. Chemiluminescence was detected under Gel Doc-XRS (Biorad) upon addition of enhanced chemiluminescence ECL kit following manufacturer's instructions.

Statistical analysis

All experiments were performed in triplicates and the results are expressed as mean ± standard deviation, unless otherwise indicated.

Acknowledgements

SP is thankful to NISER for the institutional fellowship. SSG and VBK are thankful to RGYI scheme (BT/PR6565/GBD/27/456/2012) of Department of Biotechnology, New Delhi, India. Thanks to Rishikesh Patil for NMR experiments.

References

1 J. A. McCubrey, L. S. Steelman, W. H. Chappell, S. L. Abrams, R. A. Franklin, G. Montalto, M. Cervello, M. Libra, S. Candido, G. Malaponte, M. C. Mazzarino, P. Fagone, F. Nicoletti, J. Basecke, S. Mijatovic, D. Maksimovic-Ivanic, M. Milella, A. Tafuri, F. Chiarini, C. Evangelisti, L. Cocco and A. M. Martelli, *Oncotarget*, 2012, **3**, 1068-1111.
2 J. A. McCubrey, L. S. Steelman, W. H. Chappell, S. L. Abrams, G. Montalto, M. Cervello, F. Nicoletti, P. Fagone, G. Malaponte, M. C. Mazzarino, S. Candido, M. Libra, J. Basecke, S. Mijatovic, D. Maksimovic-Ivanic, M. Milella, A. Tafuri, L. Cocco, C. Evangelisti, F. Chiarini and A. M. Martelli, *Oncotarget*, 2012, **3**, 954-987.
3 M. Marshall, *Mol. Reprod. Dev.*, 1995, **42**, 493-499.
4 K. P. Hoeflich, D. C. Gray, M. T. Eby, J. Y. Tien, L. Wong, J. Bower, A. Gogineni, J. Zha, M. J. Cole, H. M. Stern, L. J. Murray, D. P. Davis and S. Seshagiri, *Cancer Res.*, 2006, **66**, 999-1006.
5 A. Preto, J. Figueiredo, S. Velho, A. S. Ribeiro, P. Soares, C. Oliveira and R. Seruca, *J. Pathol.*, 2008, **214**, 320-327.
6 S. E. Baldus, K. L. Schaefer, R. Engers, D. Hartleb, N. H. Stoecklein and H. E. Gabbert, *Clin. Cancer Res.*, 2010, **16**, 790-799.
7 M. Beeram, A. Patnaik and E. K. Rowinsky, *J. Clin. Oncol.*, 2005, **23**, 6771-6790.
8 R. Marais, Y. Light, H. F. Paterson, C. S. Mason and C. J. Marshall, *J. Biol. Chem.*, 1997, **272**, 4378-4383.
9 J. Avruch, X. F. Zhang and J. M. Kyriakis, *Trends Biochem. Sci.*, 1994, **19**, 279-283.
10 C. Wellbrock, M. Karasarides and R. Marais, *Nat Rev. Mol. Cell Biol.*, 2004, **5**, 875-885.
11 W. De Roock, B. Claes, D. Bernasconi, J. De Schutter, B. Biesmans, G. Fountzilas, K. T. Kalogeras, V. Kotoula, D. Papamichael, P. Laurent-Puig, F. Penault-Llorca, P. Rougier, B. Vincenzi, D. Santini, G. Tonini, F. Cappuzzo, M. Frattini, F. Molinari, P. Saletti, S. De Dosso, M. Martini, A. Bardelli, S. Siena, A. Sartore-Bianchi, J. Tabernero, T. Macarulla, F. Di Fiore, A. O. Gangloff, F. Ciardiello, P. Pfeiffer, C. Qvortrup, T. P. Hansen, E. Van Cutsem, H. Piessevaux, D. Lambrechts, M. Delorenzi and S. Tejpar, *Lancet Oncol.*, 2010, **11**, 753-762.
12 A. S. Sameer, *Front Oncol.*, 2013, **3**, 114.
13 A. Thiel and A. Ristimaki, *Front Oncol*, 2013, **3**, 281.
14 S. G. Sharma and M. L. Gulley, *Arch. Pathol. Lab Med.*, 2010, **134**, 1225-1228.
15 R. Dienstmann and J. Tabernero, *Anticancer Agents Med. Chem.*, 2011, **11**, 285-295.
16 R. B. Corcoran, H. Ebi, A. B. Turke, E. M. Coffee, M. Nishino, A. P. Cogdill, R. D. Brown, P. Della Pelle, D. Dias-Santagata, K. E. Hung, K. T. Flaherty, A. Piris, J. A. Wargo, J. Settleman, M. Mino-Kenudson and J. A. Engelman, *Cancer Discov.*, 2012, **2**, 227-235.
17 H. Yang, B. Higgins, K. Kolinsky, K. Packman, W. D. Bradley, R. J. Lee, K. Schostack, M. E. Simcox, S. Kopetz, D. Heimbrook, B. Lestini, G. Bollag and F. Su, *Cancer Res.*, 2012, **72**, 779-789.
18 H. Hao, V. M. Muniz-Medina, H. Mehta, N. E. Thomas, V. Khazak, C. J. Der and J. M. Shields, *Mol. Cancer Ther.*, 2007, **6**, 2220-2229.
19 M. S. Reimers, E. C. Zeestraten, P. J. Kuppen, G. J. Liefers and C. J. van de Velde, *Gastroenterol Rep. (Oxf)*, 2013, **1**, 166-183.
20 Z. X. Yuan, X. Y. Wang, Q. Y. Qin, D. F. Chen, Q. H. Zhong, L. Wang and J. P. Wang, *PLoS One*, 2013, **8**, e65995.
21 A. Sartore-Bianchi, K. Bencardino, A. Cassingena, F. Venturini, C. Funaioli, T. Cipani, A. Amatu, L. Pietrogiovanna, R. Schiavo, F. Di Nicolantonio, S. Artale, A. Bardelli and S. Siena, *Cancer Treat. Rev.*, 2010, **36 Suppl 3**, S1-5.
22 A. S. Little, K. Balmanno, M. J. Sale, S. Newman, J. R. Dry, M. Hampson, P. A. Edwards, P. D. Smith and S. J. Cook, *Sci Signal*, 2011, **4**, ra17.
23 A. Prahallad, C. Sun, S. Huang, F. Di Nicolantonio, R. Salazar, D. Zecchin, R. L. Beijersbergen, A. Bardelli and R. Bernards, *Nature*, 2012, **483**, 100-103.
24 K. Cichowski and P. A. Janne, *Nature*, 2010, **464**, 358-359.
25 S. Whittaker, R. Kirk, R. Hayward, A. Zambon, A. Viros, N. Cantarino, A. Affolter, A. Nourry, D. Niculescu-Duvaz, C. Springer and R. Marais, *Sci. Transl. Med.*, 2010, **2**, 35-41.
26 C. Bokemeyer, E. Van Cutsem, P. Rougier, F. Ciardiello, S. Heeger, M. Schlichting, I. Celik and C. H. Kohne, *Eur. J. Cancer*, 2012, **48**, 1466-1475.
27 L. De Mattos-Arruda, R. Dienstmann and J. Tabernero, *Clin. Colorectal Cancer*, 2011, **10**, 279-289.
28 S. Ogino, K. Shima, J. A. Meyerhardt, N. J. McCleary, K. Ng, D. Hollis, L. B. Saltz, R. J. Mayer, P. Schaefer, R. Whittom, A. Hantel, A. B. Benson, 3rd, D. Spiegelman, R. M. Goldberg, M. M. Bertagnolli and C. S. Fuchs, *Clin. Cancer Res.*, 2012, **18**, 890-900.
29 R. S. Lo, *Cell Res.*, 2012, **22**, 945-947.
30. S. D. Verma, N. Pal, M. K. Singh, H. Shweta, M. F. Khan and S. Sen, *Anal. Chem.*, 2012, **84**, 7218-7226.
31. K. I. McLuckie, Z. A. Waller, D. A. Sanders, D. Alves, R. Rodriguez, J. Dash, G. J. McKenzie, A. R. Venkitaraman and S. Balasubramanian, *J. Am. Chem. Soc.*, 2011, **133**, 2658-2663.
32 D. Chadar, S. S. Rao, A. Khan, S. P. Gejji, K. S. Bhat, T. Weyhermüller and S. Salunke-Gawali, *RSC Adv*, 2015, **5**, 57917-57929.
33. L. Cincotta, J. W. Foley and A. H. Cincotta, *Cancer Res.*, 1993, **53**, 2571-2580.
34. J. Jose, A. Loudet, Y. Ueno, R. Barhoumi, R. C. Burghardt and K. Burgess, *Org. Biomol. Chem.*, 2010, **8**, 2052-2059.
35 R. Straussman, T. Morikawa, K. Shee, M. Barzily-Rokni, Z. R. Qian, J. Du, A. Davis, M. M. Mongare, J. Gould, D. T. Frederick, Z. A. Cooper, P. B. Chapman, D. B. Solit, A. Ribas, R. S. Lo, K. T.

Flaherty, S. Ogino, J. A. Wargo and T. R. Golub, *Nature*, 2012, **487**, 500-504.
36 M. J. Sale and S. J. Cook, *Biochem. J.*, 2013, **450**, 285-294.
37 L. Kathawate, P. V. Joshi, T. K. Dash, S. Pal, M. Nikalje, T. Weyhermüller, V. G. Puranik, V. B. Konkimalla and S. Salunke-Gawali, *J. Mol. Struc.*, 2014, **1075**, 397-405.
38 D. Chadar, M. Camilles, R. Patil, A. Khan, T. Weyhermüller and S. Salunke-Gawali, *J. Mol. Struc.,* 2015, **1086**, 179-189.
39 R. Patil, D.Chadar, D. Chaudhari, J. Peter, M. Nikalje, T. Weyhermüller, S. Salunke-Gawali, *J. Mol. Struc*., 2014, **1075**, 375-351.
40 N. Wagle, C. Emery, M. F. Berger, M. J. Davis, A. Sawyer, P. Pochanard, S. M. Kehoe, C. M. Johannessen, L. E. Macconaill, W. C. Hahn, M. Meyerson and L. A. Garraway, *J. Clin. Oncol.*, **29**, 3085-3096.
41 D. D. Perrin, W. L. F. Armarego and D. R. Perrin, *Pergamon Press, Oxford*, 1988, pp 260.
42 SADABS, Bruker–Siemens Area Detector Absorption and Other Correction, G.M. Sheldrick, University of Göttingen, Germany, 2006, Version 2008/1.
43 ShelXTL 6.14 Bruker AXS Inc., Madison, WI, USA 2003.
44 G. M. Sheldrick, SHELX-97 Program for crystal structure solution and refinement, University of Göttingen, Germany, 1997.
45 Y. Zhao and D. G. Truhlar, *Acc. Chem. Res.*, 2008, **41**, 157-167.
46 Y. Zhao and D. G. Truhlar, *J. Chem. Theory Comput.*, 2005, **1**, 415-432.
47 M. J. Frisch, G. W. Trucks, H. B. Schlegel, G. E. Scuseria, M. A Robb, J. R. Cheeseman, J. A. Jr. Montgomery, T. Vreven, K. N. Kudin, J. C.Burant, J. M. Millam, S. S. Iyengar, J. Tomasi, V. Barone, B. Mennucci, M. Cossi, G.Scalmani, N. Rega, G. A. J. Petersson, H. Nakatsuji, M. Hada, M. Ehara, K. Toyota, R. Fukuda, Hasegawa, M. Ishida, T. Akajima, Y. Honda, O. Kitao, H. Nakai, M. Klene, X. Li, J. E. Knox, H. P. Hratchian, J. B. Cross, V. Bakken, C. Adamo, J. Jaramillo, R. Gomperts, R. E. Stratmann, O. Yazyev, A. J. Austin, R. Cammi, C. Pomelli, J. W. Ochterski, P. Y. Ayala, K. Morokuma, G. A. Voth, P. Salvador, J. J. Dannenberg, V. G. Zakrzewski, S. Dapprich, A. D. Daniels, M. C. Strain, O. Farkas, D. K. Malick, A. D. Rabuck, K. Raghavachari, J. B. Foresman, J. V. Ortiz, Q. Cui, A. G. Baboul, S. Clifford, J. Cioslowski, B. B. Stefanov, G. Liu, A. Liashenko, P. Piskorz, I. Komaromi, R. L. Martin, D. J. Fox, T. Keith, M. A. Al-Laham, Peng, C. Y. Nanayakkara, A. Challacombe, M. Gill, P. M. W. Johnson, B. Chen, W. Wong, M. W. Gonzalez, C. Pople, J. A. *Gaussian03*, revision Gaussian, Inc.: Pittsburgh, PA, 2003.

Table 1 Crystal Structure data for **2B** and **3B**

Identification code	**2B**	**3B**
Empirical formula	$C_{17}H_{11}NO_2$	$C_{16}H_9NO_2$
Formula weight	261.27	247.24
Temperature	100(2) K	293(2) K
Wavelength	0.71073 Å	0.71073 Å
Crystal system	Monoclinic	Monoclinic
Space group	$P2_1/n$	$P\ 2_1/n$
Unit cell dimensions	a = 13.288(2) Å b = 4.6447(6) Å, β= 101.696(2)° c = 19.479(3) Å	a = 3.91910(9) Å b =23.3060(5) Å, β = 94.315(1)° c = 12.3580(3) Å
Volume	1177.3(3) $Å^3$	1125.56(4) $Å^3$
Z	4	4
Density (calculated)	1.474 Mg/m^3	1.459 Mg/m^3
Absorption coefficient	0.098 mm^{-1}	0.097 mm^{-1}
F(000)	544	512
Crystal size	0.834 x 0.072 x 0.061 mm^3	0.38 x 0.09 x 0.04 mm^3
Theta range for data collection	1.706 to 30.889°	1.75 to 23.97°
Index ranges	-19<=h<=19, -6<=k<=6, -28<=l<=28	-4<=h<=4, -26<=k<=25, -13<=l<=14-7<=h<=8, -
Reflections collected	31939	7783
Independent reflections	3718 [R(int) = 0.0516]	1766 [R(int) = 0.0473]
Completeness to theta = 25.242°	99.9 %	99.6 %
Absorption correction	Gaussian	Semi-empirical from equivalents
Max. and min. transmission	0.99490 and 0.95827	0.9961 and 0.9636
Refinement method	Full-matrix least-squares on F^2	Full-matrix least-squares on F^2
Data / restraints / parameters	3718 / 0 / 182	1766 / 0 / 209
Goodness-of-fit on F^2	1.076	1.041
Final R indices [I>2sigma(I)]	R1 = 0.0408, wR2 = 0.1144	R1 = 0.0350, wR2 = 0.0901
R indices (all data)	R1 = 0.0514, wR2 = 0.1251	R1 = 0.0508, wR2 = 0.1019
Extinction coefficient	n/a	0.015(3)
Largest diff. peak and hole	0.497 and -0.237 $e.Å^{-3}$	0.176 and -0.128 $e.Å^{-3}$

RSC Advances

ARTICLE

Table 2 Hydrogen bonding interactions in **2B** and **3B**

Com	Sr. No	D-H···A	D-H(Å)	H···A(Å)	D···A(Å)	∠D-H···A(°)
2B	1	C(13)-H(13A)···O(5)$^{(i)}$	0.980(1)	2.672 (1)	3.299(1)	122.11(8)
	2	C(13)-H(13C)···O(5)$^{(ii)}$	0.980(1)	2.654(1)	3.626(3)	171.52(8)
	3	C(3)-H(3)···O(5)$^{(iii)}$	0.951(1)	2.586(1)	3.437(1)	149.13(6)
	4	C(8)-H(8)···O(7)$^{(iv)}$	0.951(1)	2.700(1)	3.640(3)	169.92(6)
3B	5	C(3)-(H3)···O(5)$^{(v)}$	0.931(2)	2.677(1)	3.362(2)	131.0(1)
	6	C(8)-(H8)···O(5)$^{(v)}$	0.930(2)	2.675(1)	3.564(2)	160.2(1)
	7	C(6)-(H6)···O(7)$^{(v)}$	0.930(1)	2.657(1)	3.560(2)	163.9(1)

(i) -1/2+x,1.5-y,-1/2+z ; (ii) -1/2+x, 2.5-y,-1/2+z; (iii) 1.5-x,-1/2+y,1/2-z; (iv) 2-x,1-y,-z ; v) 1-x,-y,2-z

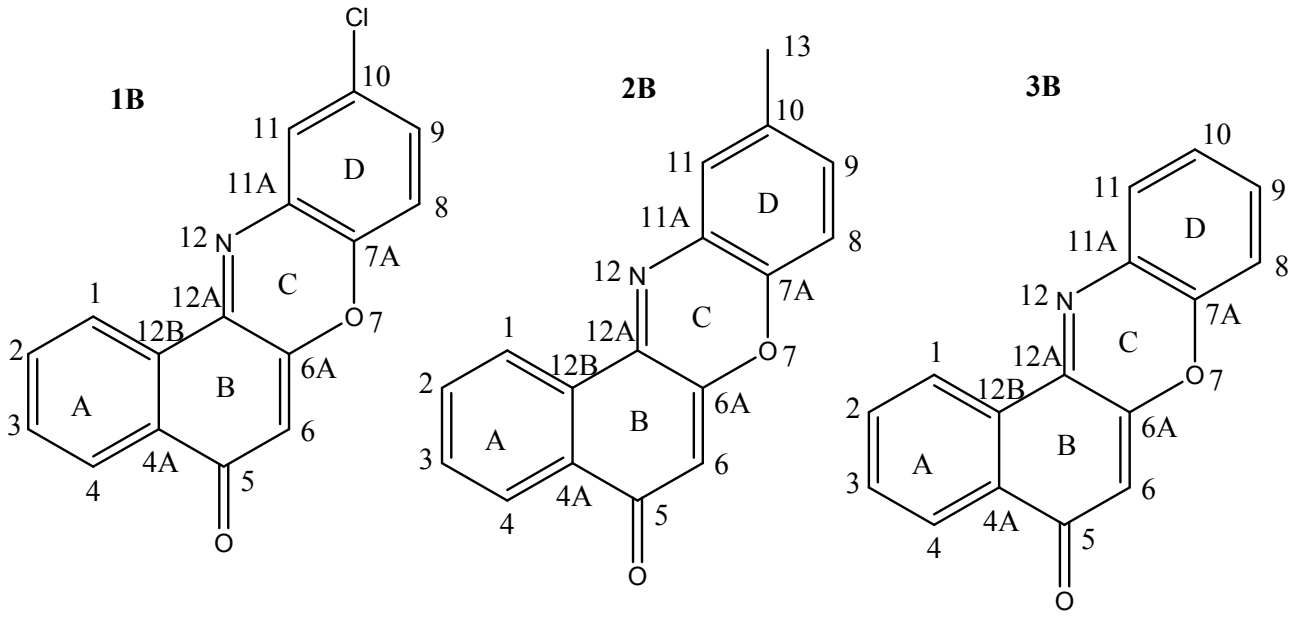

Scheme 1 Molecular structure of **1B**, **2B** and **3B.**

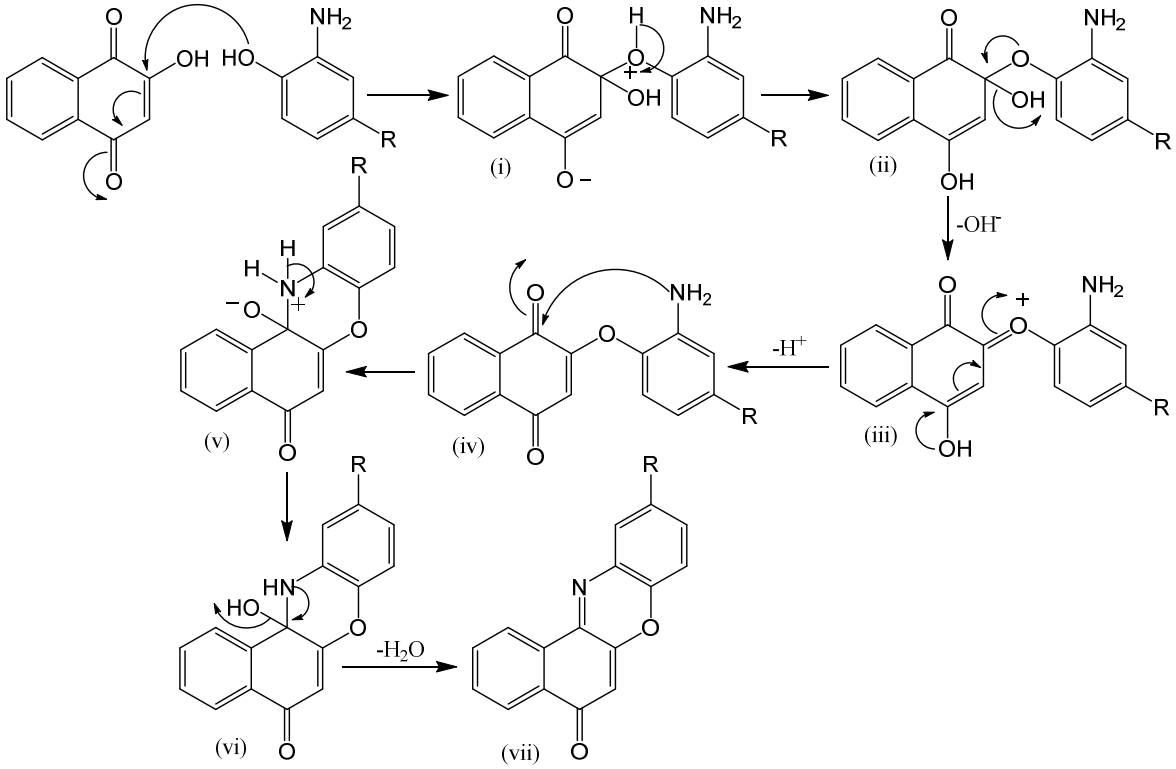

Scheme 2 Reaction mechanism involved in the synthesis of **1B** to **3B.**

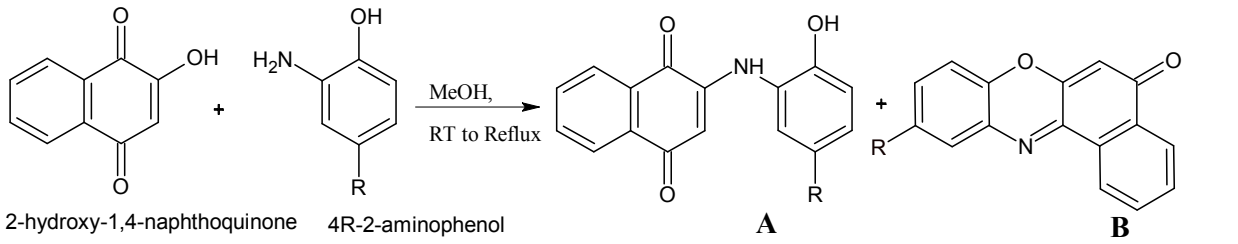

2-hydroxy-1,4-naphthoquinone

4R-2-aminophenol

2-[(4R-hydroxyphenyl)amino] naphthalene-1,4-dione

R= **1A**;Cl, **2A**;CH_3, **3A**; H

[10R-benzo[α]phenoxazine]-5-one

R=**1B**; Cl, **2B**; CH_3 **3B**;H

Scheme 3 General reaction scheme for synthesis of **1B**, **2B** and 3B**.**

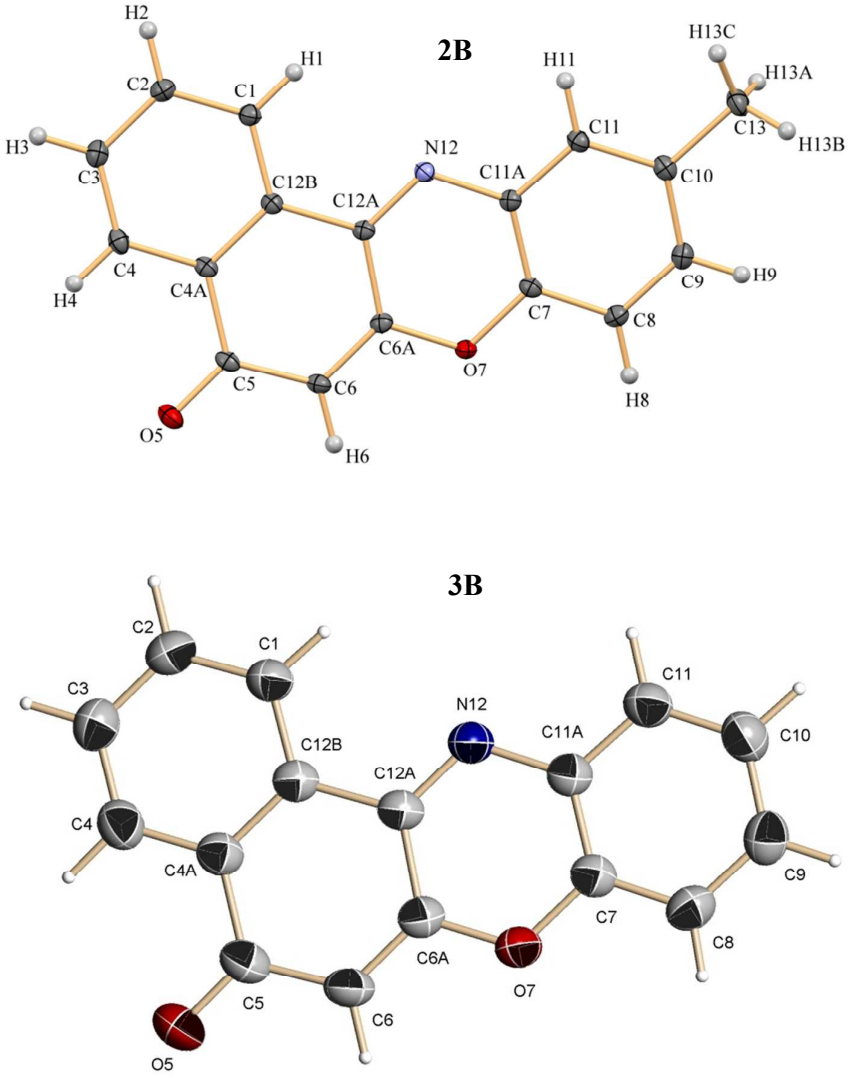

Fig. 1 ORTEP plot of **2B** and **3B** the ellipsoid was drawn with 50% probability.

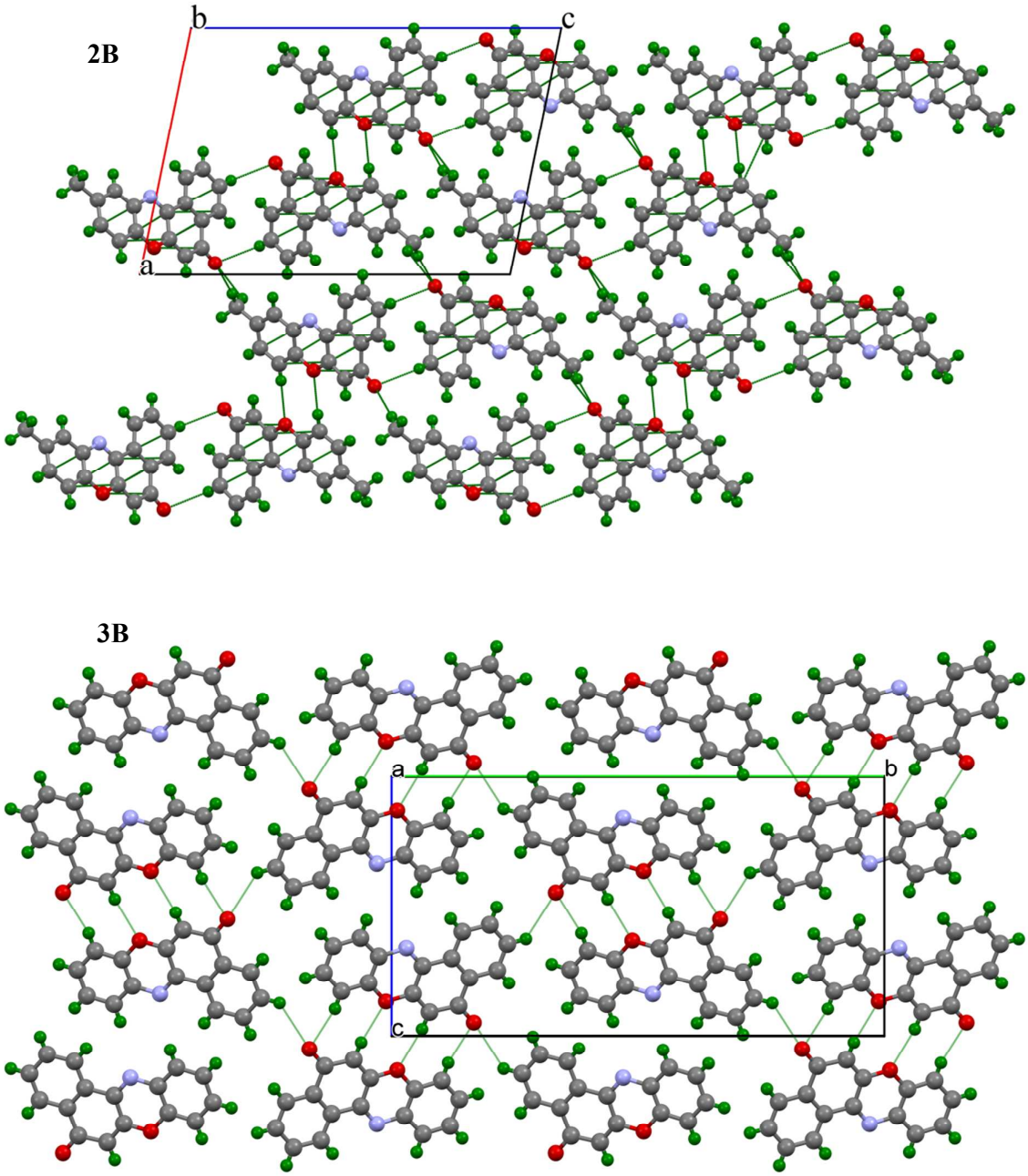

Fig. 2 Molecular packing of **2B** down 'b'-axis(top) and for **3B** down 'a'-axis(bottom).

a)

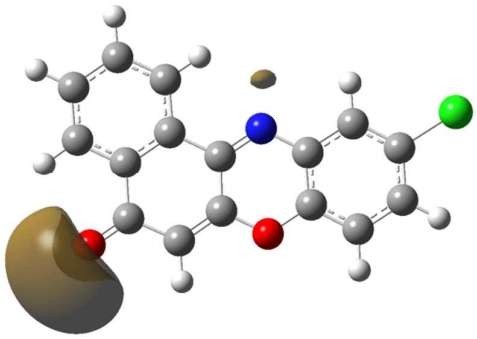

b)

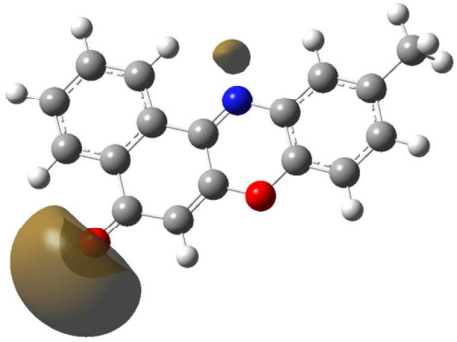

c)

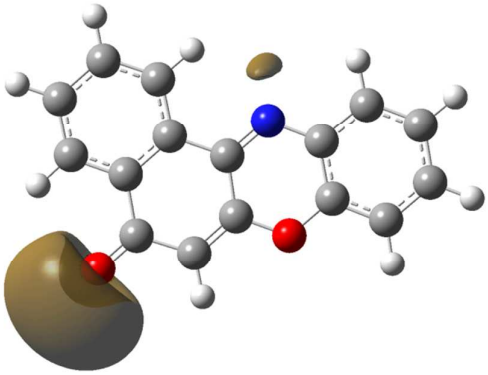

Fig.3 Molecular electrostatic potential surface (0.02 a.u isosurface) in (a) **1B** (b) **2B** and (c) **3B**.

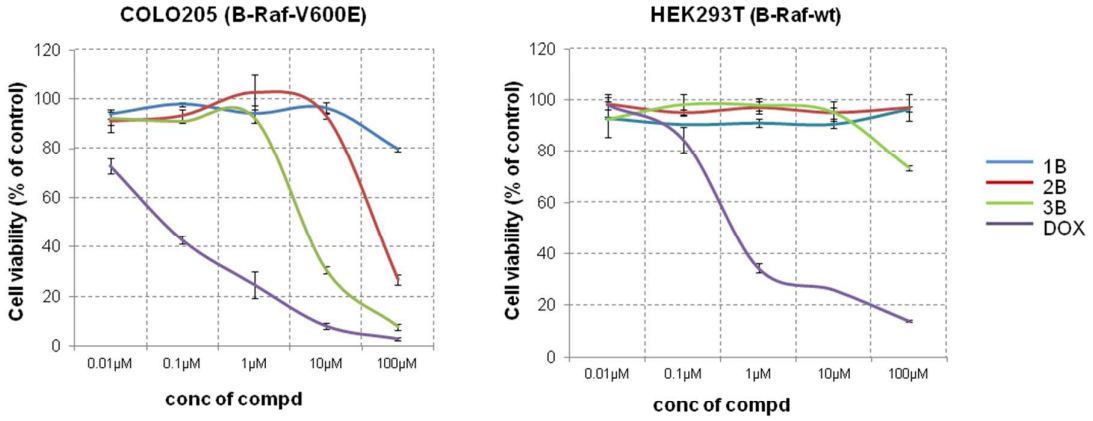

		1B	2B	3B	DOX
Malignant Cell line (COLO205)	IC_{50}	>100 μM	13 μM	9 μM	68 nM
	Doses used	50 μM	13 μM	9 μM	100 nM
	Remarks	inactive	active	active	positive control
Non-malignant cell line (HEK293T)	IC_{50}	>100 μM	>100 μM	>100 μM	0.33 μM
	Doses used	50 μM	50 μM	50μM	0.77 μM
	Remarks	inactive	inactive	inactive	positive control

Fig. 4 Dose-dependent cell viability data for compounds **1B**, **2B** and **3B** upon treatment in COLO205 and HEK293T cells for 72 h. Results (n=3) are expressed as mean ± SD and IC_{50} doses were determined for bioactive compounds. The doses that were used for further studies IC_{50} value for bioactive compounds or 50μM for inactive compound are shown in the panel below. Doxorubicin (DOX) has been used as positive control.

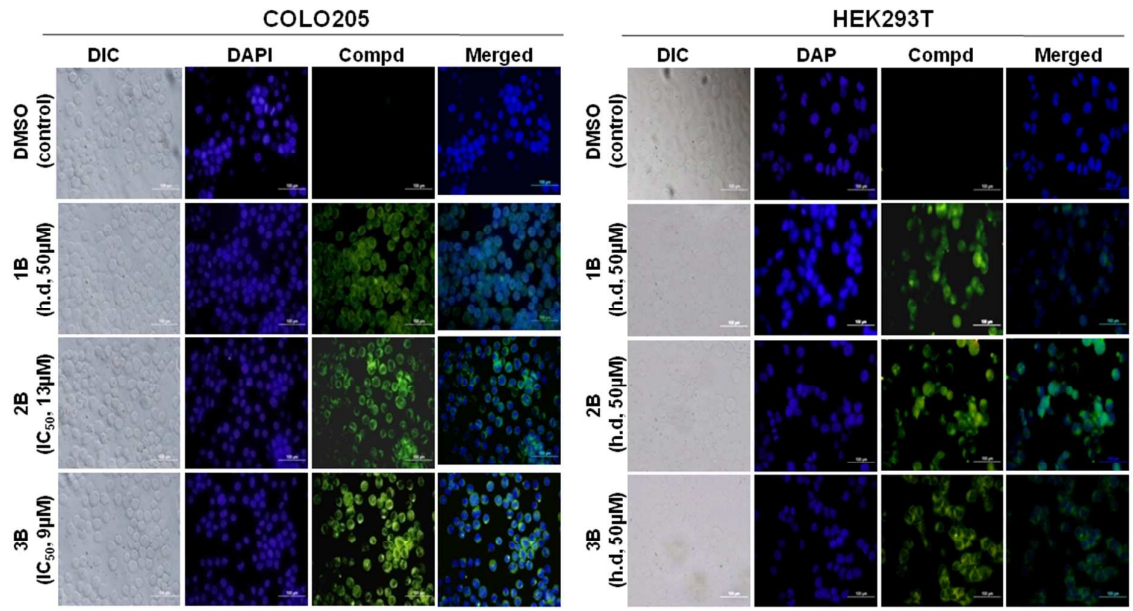

Fig. 5 Cell permeability studies for compounds **1B**, **2B** and **3B** using fluorescence microscopy within 15mins post exposure. COLO205 and HEK293T were incubated with compounds (**1B**, **2B** and **3B**) at above mentioned concentrations for 15 mins. Cytosolic accumulation of compounds (*green fluorescence*) was confirmed when nucleus was counter-stained (*blue color*) with DAPI. The cells were either treated with their respective IC_{50} concentrations or high dose of 50 μM for inactive compounds.

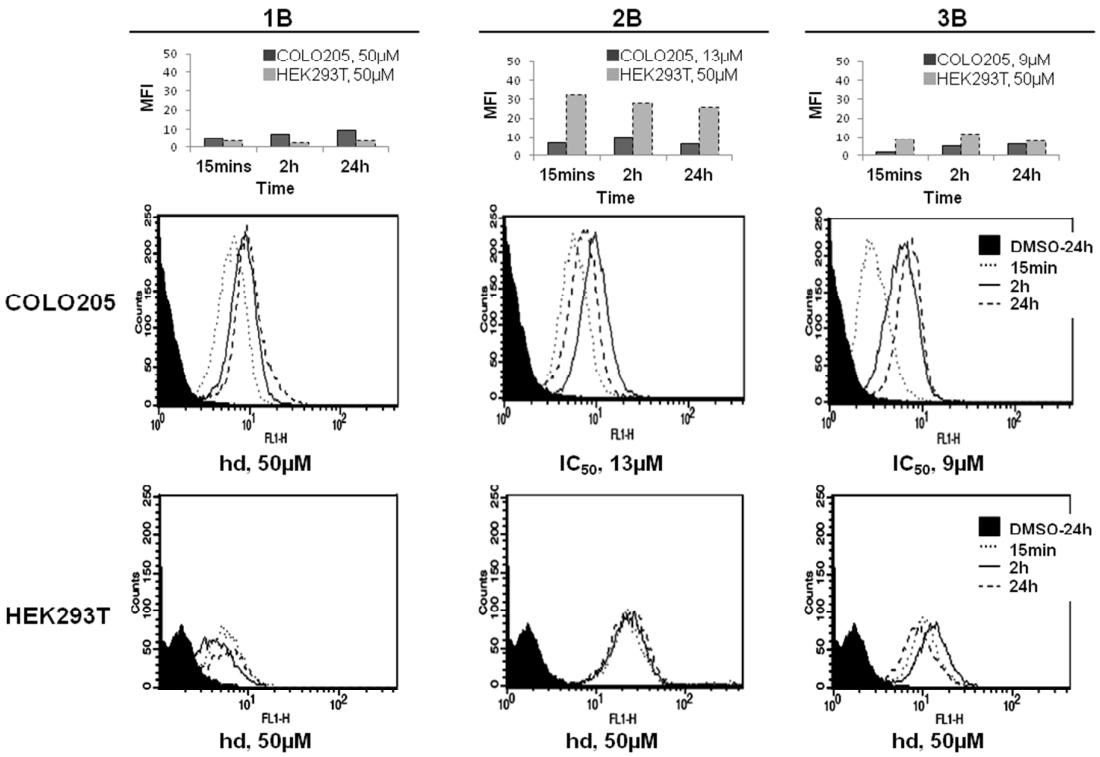

Fig. 6 Flow cytometric analysis for cellular uptake of compounds (at 15min, 2h and 24h post treatment) in COLO205 and HEK293T. The extent of cellular uptake in terms of mean fluorescence intensity (MFI) show that HEK293T cells were more refractory towards all three compounds even at high doses (h.d, 50µM) as compared to COLO205 where compound **1B** was treated at high dose of 50µM and both **2B** and **3B** were treated at their IC_{50} doses.

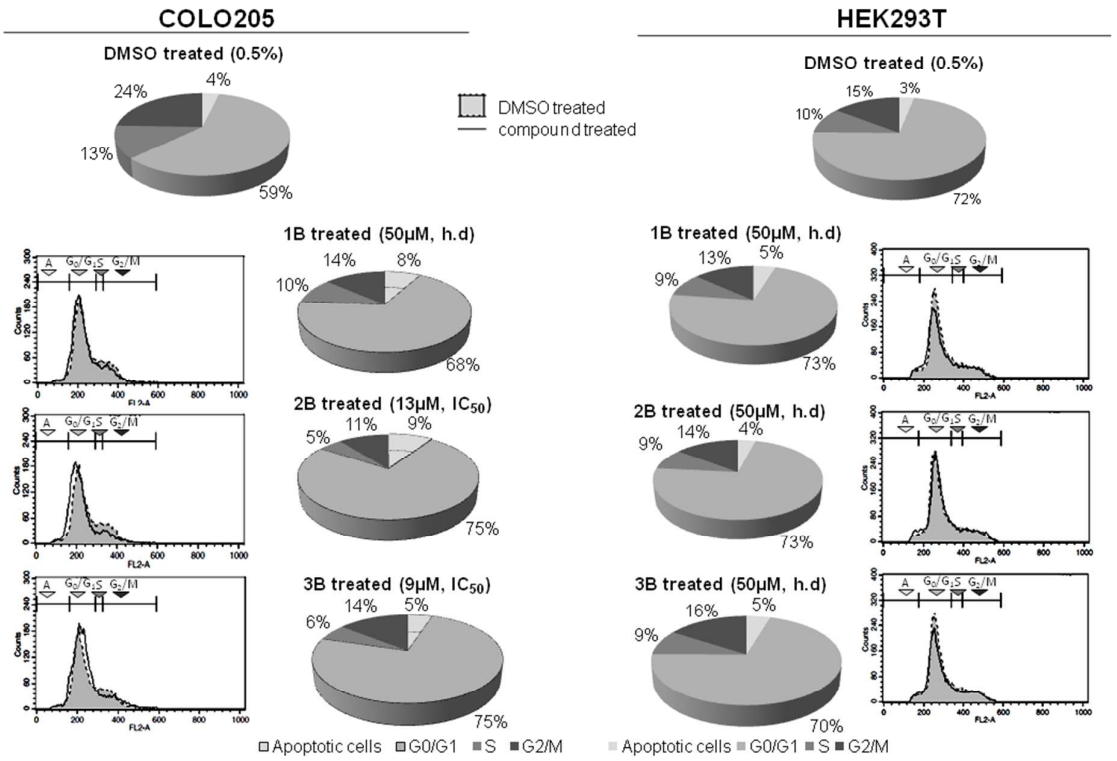

Fig. 7 Propidium iodide staining for cell cycle studies using flow cytometry. G_0/G_1 phase arrest in cell cycle was observed in COLO205 cells (*left panel*). Compounds **2B** and **3B** were able to show equivalent activity at IC50 concentrations 5 times lower than that of compound **1B**. No cell cycle arrest was observed in HEK293T cells (*right panel*) with compounds even when treated at a high dose (h.d.) of 50 μM.

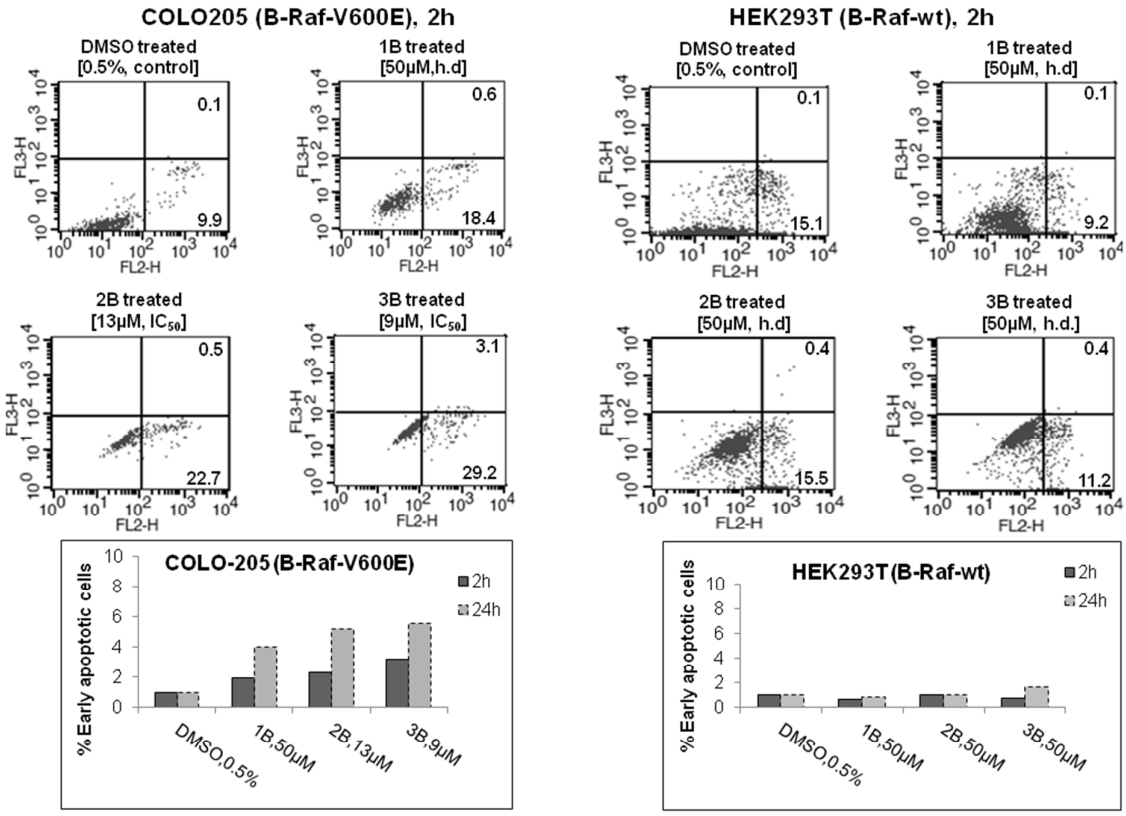

Fig. 8 Annexin-V assay for assessment of apoptotic activity in **1B**, **2B** and **3B** treated COLO205 and HEK293T cells. Apoptosis was determined after treating both cell lines with compounds **1B**, **2B** and **3B** followed by staining with Annexin-V/7-AAD after 2h (*top*). Flow cytometry profile (scatter plots, *top panel*) represents Annexin-V-PE staining in *x-axis* (FL2-H) and 7-AAD in *y-axis* (FL3-H). Histograms for early apoptosis after 2h and 24h are expressed in percentage in each experimental condition (*lower panel*).

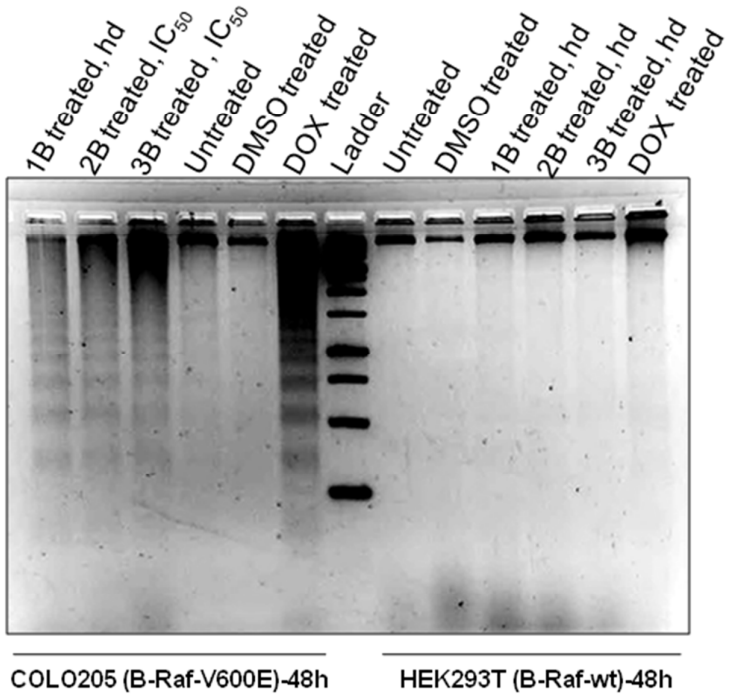

Fig. 9 Compounds **1B**, **2B** and **3B** induced DNA fragmentation only in COLO205 (BRAF V600E) colon cancer cells**.** After 48h treatment of both HEK293T and COLO205 cells with compounds **1B**, **2B** and **3B** at indicated doses (high dose of 50 μM for inactive and IC_{50} dose for active compound), the chromosomal DNA was extracted. On a 1.8% agarose gel, DNA laddering profile was observed in COLO205 (BRAF V600E) cell lines when treated with compounds **1B**, **2B** and **3B** for 48h indicate stronger apoptotic activity. This was not observed in HEK293T cells where the BRAF is wild-type.

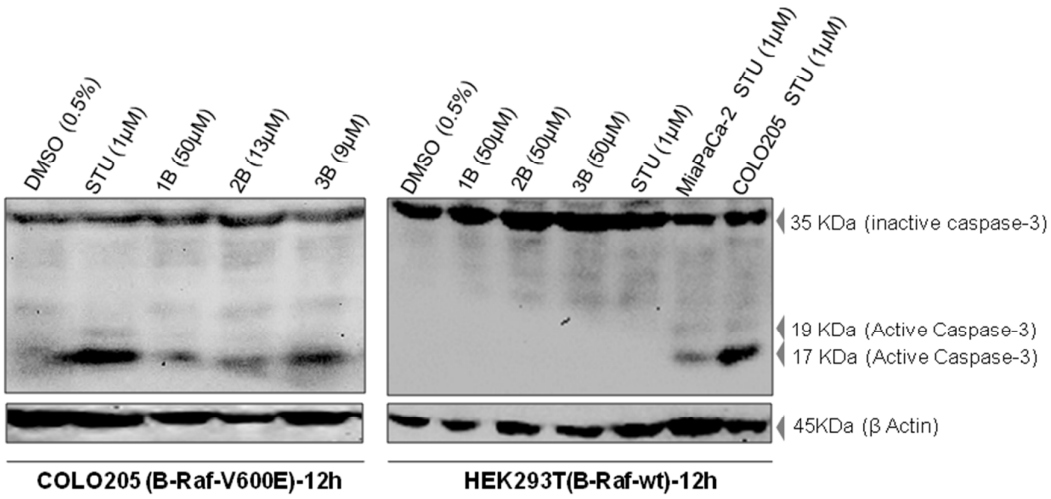

Fig. 10 Compounds **1B**, **2B** and **3B** induced Caspase-3 dependent apoptosis in COLO205 (BRAF V600E) cells. Caspase-3 activation by compounds **1B**, **2B** and **3B** after 12 hours of treatment was detected (17kDa band) with primary antibody (anti-human caspase3 at 1:1000 dilution) and anti-human β-actin at 1:1000 dilution was used to detect β-actin that was used as loading control. 1μM Staurosporine (STU) treated cell lysates were used as positive control.

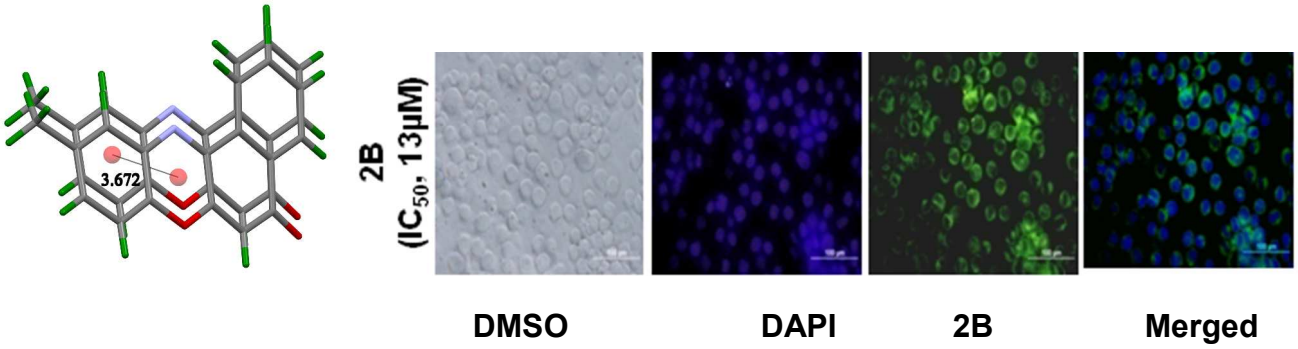

Benzo[α]phenoxazine derivative specifically toxic to malignant COLO205 cell line with BRAF mutation (V600E) and nontoxic to non-malignant wild-type BRAF HEK293T cell line